Frontiers in Bioscience Landmark

Front. Biosci. (Landmark Ed) **2024**; 29(3): 104
https://doi.org/10.31083/j.fbl2903104

Original Research

NOP14 as a Potential Predictor of Adult-Type Diffuse Glioma Prognosis and Immunotherapy, is Related to Cell Migration, Proliferation, and CD8$^+$T Cell Infiltration

Qiu-si Tian[1], Jing Cheng[2], Zhi-jun Bao[1,*]

[1]Department of Neurosurgery, 3201 Hospital of Xi'an Jiaotong University Health Science Center, 723000 Hanzhong, Shaanxi, China
[2]Department of Pathology, 3201 Hospital of Xi'an Jiaotong University Health Science Center, 723000 Hanzhong, Shaanxi, China
*Correspondence: baozhijun3201@163.com (Zhi-jun Bao)

Academic Editor: Pier Paolo Piccaluga
Submitted: 22 November 2023 Revised: 3 January 2024 Accepted: 24 January 2024 Published: 15 March 2024

Abstract

Background: World Health Organization (WHO) grade 4 adult-type diffuse glioma is the most malignant primary tumor of the brain. Nucleolar protein 14 (*NOP14*) is recognized to contribute significantly to the assembly of small ribosomal subunits. However, the specific involvement of NOP14 in diverse cancers remains poorly understood, particularly its role in adult-type diffuse glioma, which has yet to be elucidated. **Methods**: A total of 20 adult-type diffuse glioma samples with varying WHO stages were collected. The protein level of NOP14 was detected using immunohistochemistry. Additionally, NOP14 expression in LN229 and U251 cell lines and collected clinical tissue samples was quantified using the Western blot technique. Furthermore, the correlation between *NOP14* and clinicopathological features, survival rates, matrix and immune scores, and immune components was investigated using data from the Cancer Gene Atlas database. **Results**: *NOP14* exhibited high expression in adult-type diffuse glioma patients, with the highest expression observed in the LN229 cell line. Moreover, elevated *NOP14* expression was significantly correlated with poorer overall survival and demonstrated an association with unfavorable pathological features in a cohort of 703 glioblastoma (GBM) patients. Evidence of a connection between *NOP14* and the tumor microenvironment was presented. Elevated *NOP14* was linked to the infiltration of CD8$^+$T cell and factors related to epithelial-mesenchymal transition. In *in vitro* assay, *NOP14* was capable of suppressing adult-type diffuse glioma cell invasion and metastasis. **Conclusions**: *NOP14* holds great promise as a candidate biomarker for detecting prognostic, molecular, and immune signatures of adult-type diffuse glioma.

Keywords: *NOP14*; glioblastoma; tumor-infiltration; prognosis; CD8$^+$T cell

1. Introduction

Approximately 80% to 85% of malignant brain tumors in adults are gliomas [1]. Gliomas exhibit a diffuse infiltration of the brain parenchyma, with an annual incidence of approximately 6.4 per 100,000 people [2]. The World Health Organization (WHO) Classification of central nervous system (CNS) tumors, Version 5, serves as an international standard for the classification of brain and spinal cord tumors. In this classification, adult diffuse gliomas are identified as a specific type [3]. Among these gliomas, WHO grade 4 adult diffuse glioma represents the most malignant type of primary brain tumor. Unfortunately, even with the current standard therapy (consisting of maximum surgical resection and concurrent chemotherapy with temozolomide), the median survival remains less than 15 months [3].

The human nucleolar protein 14 (*NOP14*) gene, located on chromosome 4p16.317, encodes a nuclear protein that is responsible for processing 18s ribosomal RNA precursors, maturation, and synthesizing 40s ribosomal subunits [4]. Milkereit *et al*. [5] discovered that the depletion of *NOP14* expression led to a decrease in the number of 20s versus 27sA2 ribosomal RNA precursors while causing an increase in the levels of 35s versus 23s precursor ribosomal RNA. Furthermore, Kühn *et al*. [6] demonstrated that the *NOP14* protein facilitated the incorporation of Noc4p into processing bodies of the ribosomal small subunit by forming a complex with *Noc4p-NOP14p*. This complex then actively participated in the processing and maturation of the ribosomal small subunit and ribosomal RNA [6].

Previous studies have demonstrated the association between *NOP14* and the occurrence, development, invasion, and metastasis of breast cancer, melanoma, straight colon cancer, and pancreatic cancer [7–10]. Despite this, little research has been conducted on the role of *NOP14* in adult-type diffuse glioma. Du *et al*. [7] discovered that *NOP14* was upregulated in pancreatic ductal adenocarcinoma (PDAC) and metastatic tissues. They identified mutp53 as a functional target of *NOP14* and showed that upregulation of *NOP14* increased mutp53 mRNA stability, promoting tumor invasion and metastasis. Additionally, *NOP14* overexpression stimulated cell motility, while its inhibition reduced the invasive capacity of PDAC cells. *NOP14* has been identified as one of the hub genes and a potential biomarker for colorectal cancer development [8].

On the other hand, Meng *et al.* [8] demonstrated the down-regulation of *NOP14* in invasive breast cancer, inhibiting its progression. Similarly, *NOP14* has been found to suppress the function and stemness of melanoma stem-like cells by inactivating the Wnt/beta-catenin signaling pathway [9,10]. Hence, the function of *NOP14* appears to vary depending on the specific type of cancer, acting as an oncogene in some tumors and a tumor suppressor gene in others. Nonetheless, the precise function and mechanism of *NOP14* in human malignant tumors, including its correlation with prognosis and immune infiltration in glioma, remain largely unknown, establishing the need for further exploration.

Our study elucidates the crucial role of *NOP14* in facilitating invasion and migration *in vitro* while also revealing the perturbed immune status in adult-type diffuse glioma, characterized by the exclusion of $CD8^{+}$T cells. Thus, *NOP14* could potentially serve as both a novel therapeutic target and a prognostic biomarker for adult-type diffuse glioma.

2. Materials and Methods

2.1 Clinical Data Collection and Screening

Twenty adult-type diffuse glioma specimens were collected through surgical resection at the 3201 Hospital, Affiliated with Xi'an Jiaotong University, from January 2021 to July 2022. The tissue specimens were routinely fixed in 10% neutral formalin and subsequently embedded in paraffin. Screening criteria: ① Patients with an initial diagnosis of glioma; ② Patients with no prior history of other associated malignancies or surgeries; ③ Patients with relatively comprehensive pathology-related data.

The study received approval from the Ethics Committee of the 3201 Hospital (approval number 2022082). All participants provided written informed consent. The clinical characteristics of the patients are presented in **Supplementary Table 1**.

2.2 Western Blot

Four fresh adult-type diffuse glioma tissues and four non-tumor brain tissue specimens obtained through internal decompression of brain injury were collected as controls. All samples were stored according to the standard in a liquid nitrogen tank for 40 minutes *in vitro*. Protein extraction was conducted, followed by the concentration determination utilizing the bicinchoninic acid assay (BCA) method. The denatured protein was placed on ice and subjected to electrophoresis. Then, the membrane was probed with the *NOP14* primary antibody (1:2000, Proteintech Group, Rosemont, IL, USA) and β-actin primary antibody (1:2000, Proteintech Group) overnight. After Smembrane washing, the corresponding rabbit and rat secondary antibody (1:2000, Proteintech Group) was added for further incubation. Following a 2-hour incubation at room temperature, the Enhanced ChemiLuminescence (ECL) chemiluminescent solution was added, and the exposure was performed using a Bio-Rad chemiluminometer (thermofisher.cn).

2.3 Immunohistochemical Analysis

All adult-type diffuse glioma samples were prepared following standard procedures, completely fixed with 10% neutral formalin, dehydrated, embedded, and then continuously sectioned at a thickness of 3 µm. The sections were dried and subjected to pretreatment using a DAKO PT Link automated immunohistochemical preconditioning system. Then, the sections were treated utilizing an AutostainerLink 48 (agilent.com.cn) fully automated immunohistochemical staining instrument. The rabbit monoclonal antibody against *NOP14* (1:2000, Proteintech Group) was acquired from Proteintech Group Company. For external control, HepG2 cells were utilized as the positive control, phosphate-buffered saline (PBS) was substituted for the primary antibody as the negative control (NC), and red blood cells within the blood vessels served as the internal control.

2.4 The NOP14 Expression and the Clinical Dataset

The mRNA expression data of *NOP14* and clinical data of glioblastoma (GBM) patients were obtained from the TCGA database (https://cancergenome.nih.gov/), and the data was processed utilizing R software (v3.6.3) and Perl (R Foundation for Statistical Computing, Vienna, Austria). The dataset included 701 patients diagnosed with GBM and 5 normal brain tissue samples. The glioma patients were categorized into high-expression and low-expression groups based on the median *NOP14* mRNA expression.

2.5 Correlation Analysis between NOP14 Expression with Clinicopathological Parameters and Prognosis

The Strawberry Perl software integrated the *NOP14* expression data from the TCGA-GBM dataset with tumor stage, histological grade, tumor size, and survival time of patients with GBM. The relationship between *NOP14* and tumor stage was tested utilizing the Kruskal (KS) test. The difference in survival between high and low *NOP14* expression groups was evaluated utilizing the Kaplan-Meier method. The predictive value of *NOP14* was assessed utilizing multivariate Cox regression.

2.6 NOP14 Single-Gene Enrichment Analysis

The gene expression data was classified into high and low groups using the median value of *NOP14* expression in the TCGA-GBM dataset. Gene Set Enrichment Analysis (GSEA) software (gsea-msigdb.org) was utilized for c2.cp.Kegg.v7 in Molecular Tabel database (Molecular Signature Database, Msig-DB). The 2.symbols.gmt data set was utilized as a set of functional genes for conducting a signaling pathway enrichment analysis of *NOP14*. The single gene enrichment results of *NOP14* were filtered based on the absolute normalized enrichment score (NES) values of 1. O, NOM p-val <0.05 and False Discovery Rate (FDR) q-val <0.25.

2.7 TIMER Database Analysis

The relationship between *NOP14* expression and the extent of immune cell infiltration, including neutrophils, macrophages, B cells, $CD4^+$T cells, $CD8^+$T cells, and dendritic cells, was explored with the help of the gene modules available in the TIMER database. Furthermore, the correlation module was adopted to analyze the association between *NOP14* expression and the expression of cell markers related to immune cell infiltration. At 0.1 or 1.0, $p < 0.05$ indicates statistical significance.

2.8 The Expression of NOP14 in Each Cell within the Microenvironment of GBM

The Tumor Immune Single-cell Hub (TISCH) database (http://tisch.comp-genomics.org/) integrated single-cell sequencing data from 27 cancers [11]. In this study, the Glioma_GSE148842 dataset was selected to test the *NOP14* expression in individual cells within the GBM microenvironment, with the results visualized using a heatmap.

2.9 Cell Culture and the Realtime Fluorescence Quantitative Polymerase Chain Reaction (qPCR) Experiments

Human normal astroglial cells (HA1800) were grown in an RPMI 1640 medium containing 10% fetal calf serum (FCS). Human glioma cell lines U87, U251, and LN229 were cultivated in high glucose Dulbecco's Modified Eagle Medium (DMEM) with 10% FCS. All cell lines were validated by short tandem repeat (STR) profiling and tested negative for mycoplasma. All cells were kept at 37 °C with 5% CO_2 and 95% humidity. Human glioma cell lines (LN229) and (U251) were purchased from Catalpa chinensis (Wuhan, China), and no mycoplasma (Myco-Zero ™ Mycoplasma removal reagent (Beyotime, Shanghai, China)). RNA extraction was implemented upon 80% confluency. RNA extraction was carried out using the Mabio RNT412-02 RNA extraction kit (vazyme.com), followed by reverse transcription using the Vazyme R222-01 kit (vazyme.com). ChamQ Universal SYBR qPCR Master Mix (Vazyme Q711-03) was chosen for qPCR analysis. The primers (synthesized by Shanghai Qingke) and cells were provided by the Biochemistry Laboratory of Chongqing University. Primer sequence:

NOP14 F: 5′-GAAGGCCAACTCCAATCCGTT-3′, R: 5′-AAGTCTGTGTACGCTTCCTGA-3′; GAPDHF: 5′-TCACCAGGGCTGCTTTTA-3′ and R: 5′-TTCACACCCATGACGAACA-3′.

2.10 Cell Transfection

The cells were seeded into six-well cell culture plates one day prior to transfection, with a density of 6×10^5 cells per well. Upon 80% confluency, cell transfection was conducted following the instructions of the Lipofectamine™3000 transfection kit (thermofisher.cn). NC cells were transfected with NC Small interfering RNA (siRNA) (NC). Cells in the siRNA-*NOP14* group were transfected with *NOP14* siRNA (*NOP14*-Si), and those in the blank control group were not transfected. After 8 hours of transfection, the regular medium containing 10% fetal bovine serum was replaced. Cell transfection efficiency was assessed by measuring the levels of *NOP14* in cells with the help of quantitative reverse transcription polymerase chain reaction (qRT-PCR) and Western blot, respectively.The *NOP14* interference sequence was designed by Ying *et al*. [12]. The *NOP14*-si1 sequence: 5′-CCAGUGACCCUGAGAGCAATT-3′, and the *NOP14*-si2 sequence: 5′-GGUUUAUACCUGAGCUUAUTT-3′, were synthesized by Shanghai Engine Biotech. The NC-siRNA sequence was 5′-CCGGGAACTCGAGT-3′.

2.11 Cell Wound Scratch Assay

Cells from the NC and *NOP14*-siRNA groups were seeded onto 6-well plates and cultured at 37 °C in a 5% CO_2 incubator. Cell fragments were eliminated by washing with PBS, and the serum-free culture medium was collected from the same field at 0 hours, 24 hours, and 48 hours, followed by cell migration calculation.

2.12 Transwell Assays

The cells were washed twice with PBS and subjected to serum-free DMEM starvation for 12 hours. The treated cells were harvested utilizing trypsin digestion. A single-cell suspension was then prepared and seeded in the Transwell upper chamber (8 µm, 24-well insert; 5×10^3 cells per well; Transwell; Corning, NY, USA). A total volume of 600 µL of complete culture medium was supplemented to the lower chamber and incubated for 24 hours. Subsequently, the chambers were removed, and non-migrated cells were discarded. The remaining cells were fixed in 4% paraformaldehyde for 10 minutes. After air-drying, the cells were stained with crystal violet and examined under a light microscope for quantification.

2.13 Clone Formation Assay

Single-cell suspensions of the NC, *NOP14*-si1, and *NOP14*-si2 groups were seeded in 6-well plates (1000 cells per well). The cells were cultured in the incubator for 10 days after 24 hours. After fixation with 4% paraformaldehyde, the cells were counterstained with crystal violet. Clones of 50 cells were observed and counted under a microscope to construct the growth curve.

2.14 Statistical Analysis

The statistical significance of the included data was determined by employing either Student's *t*-test (for pairwise comparisons) or two-way ANOVA (for comparisons between multiple groups). Data are presented as fold-changes, reported as mean ± Structural Equation Modeling (SEM) or ± Standard Deviation (SD). Significant differences were determined using a *p*-value < 0.05 threshold.

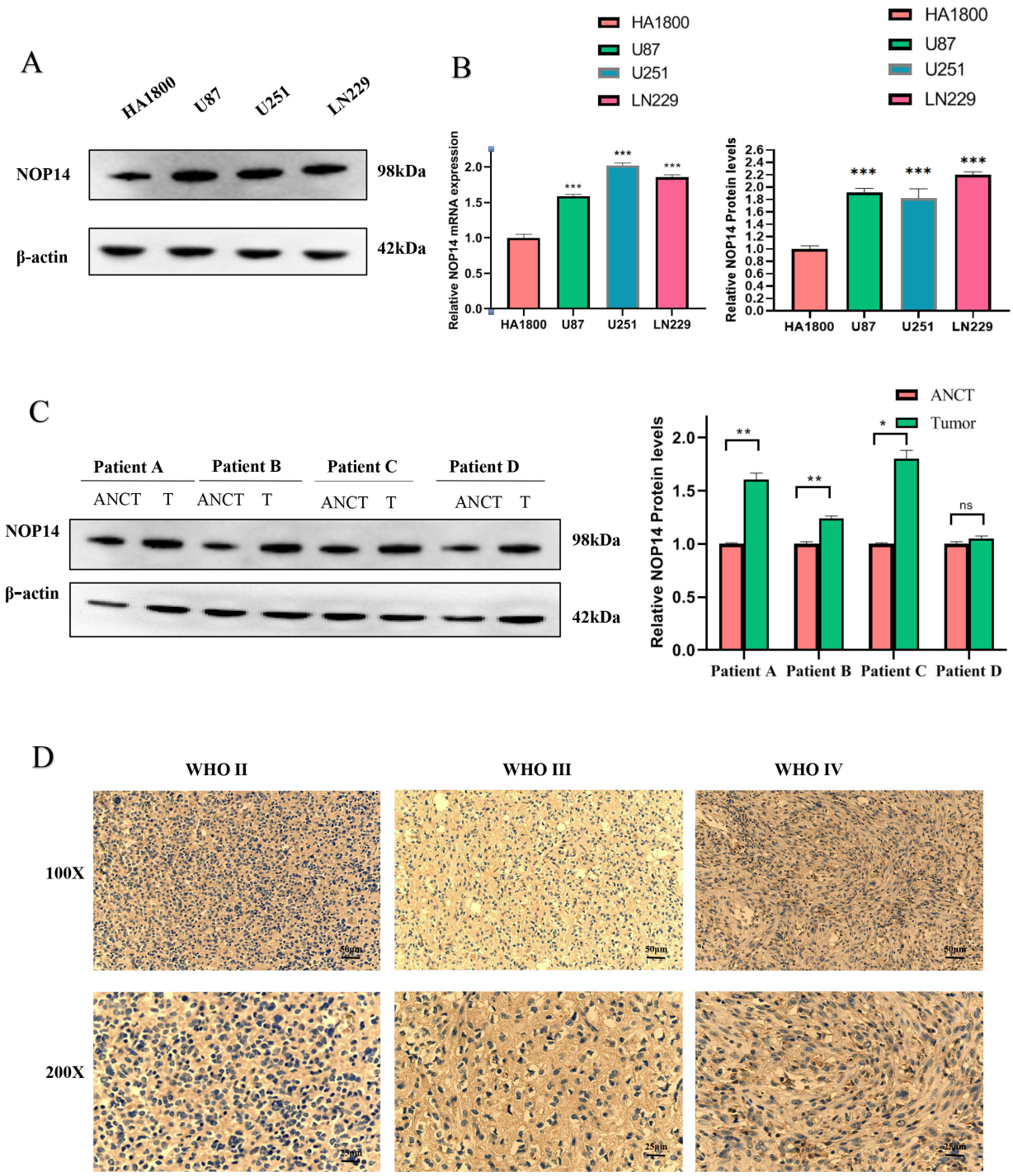

Fig. 1. The *nucleolar protein 14* (*NOP14*) expression is upregulated in the Glioma. (A) Western Blot for the expression of *NOP14* protein in several different glioma cell lines and normal astrocytes. (B) Quantitative map of *NOP14* mRNA expression and protein expression. (C) Western blotting detection of Glioma clinical adjacent four cases of benign and cancer tissue. (D) Quantitative map of *NOP14* protein expression; Immunohistochemical detection of *NOP14* expression of different grades. *** $p < 0.001$, ** $p < 0.01$, * $p < 0.05$, ^{ns} $p \geq 0.05$. ANCT, Adjacent Non-Cancerous Tissue; WHO, The World Health Organization.

3. Results

3.1 NOP14 is Highly Expressed in GBM Cells and Tissues

As illustrated in Fig. 1A,B, the expression of *NOP14* was markedly elevated in glioma cell lines (U87, U251, LN229) compared to the normal astrocyte HA1800 (Fig. 1A,B). Similarly, tissue samples collected from 4 cases exhibited a high *NOP14* in tumor tissue (Fig. 1C,D). Moreover, we tested *NOP14* expression in various grades of

Table 1. Demographic and clinicopathological parameters of high and low *NOP14* expression group patients with Glioma in The cancer genome atlas (TCGA).

Characteristic	Low expression of *NOP14*	High expression of *NOP14*	*p*
n	348	348	
WHO grade, n (%)			<0.001
G2	159 (25%)	65 (10.2%)	
G3	115 (18.1%)	128 (20.2%)	
G4	40 (6.3%)	128 (20.2%)	
IDH status, n (%)			<0.001
Wild-type (WT)	81 (11.8%)	165 (24.1%)	
Mut	262 (38.2%)	178 (25.9%)	
1p/19q codeletion, n (%)			<0.001
Codel	120 (17.4%)	51 (7.4%)	
Non-codel	227 (32.9%)	291 (42.2%)	
Gender, n (%)			0.491
Female	144 (20.7%)	154 (22.1%)	
Male	204 (29.3%)	194 (27.9%)	
Primary therapy outcome, n (%)			0.244
PD	57 (12.3%)	55 (11.9%)	
SD	87 (18.8%)	60 (13%)	
PR	41 (8.9%)	23 (5%)	
CR	86 (18.6%)	53 (11.5%)	
Age, n (%)			<0.001
≤60	300 (43.1%)	253 (36.4%)	
>60	48 (6.9%)	95 (13.6%)	
Histological type, n (%)			<0.001
Astrocytoma	105 (15.1%)	90 (12.9%)	
Glioblastoma	40 (5.7%)	128 (18.4%)	
Oligoastrocytoma	81 (11.6%)	53 (7.6%)	
Oligodendroglioma	122 (17.5%)	77 (11.1%)	
Age, median (IQR)	41 (33, 53)	50 (36, 62)	<0.001

WHO, World Health Organization; IDH, Isocitrate Dehydrogenase; PD, progressive disease; SD, stable disease; PR, partial response; CR, complete response; IQR, Interquartile Range.

glioma (n = 20). As the glioma grade level increased, there was an observed increase in *NOP14* expression in glioma immunohistochemical staining. Our results showed a significant upregulation of *NOP14* expression in glioma tissues compared to non-glioma tissues (all $p < 0.05$).

3.2 Clinical Characteristics and Survival Prognosis

Table 1 summarizes the clinical data of the 696 GBM patients. In this study, a total of 398 men and 298 women were analyzed. The chi-square test results demonstrated a significant correlation between *NOP14* and WHO grade, isocitrate dehydrogenase (IDH) status, 1p/19q codeletion, and histological type (all $p < 0.001$). The Wilcoxon rank-sum test revealed a significant association between *NOP14* and age ($p < 0.001$). There was no significant association between *NOP14* expression and other clinicopathological features.

3.3 Correlation Analysis of NOP14 Expression and Clinicopathological Characteristics

The expression of *NOP14* was analyzed in patients with various clinicopathological features in this study. Among them, Levene's test of homogeneity of variance and one-way ANOVA test showed that the expression of *NOP14* mRNA increased with the WHO level (Fig. 2A). Moreover, *NOP14* was differentially expressed regarding the primary therapy outcome for glioma and the histological type (Fig. 2B,C). The Mann-Whitney U test analysis revealed a higher expression of IDH wild-type compared to mutant *NOP14* mRNA (Fig. 2D), non-codel 1p/19 compared to codel (Fig. 2E). Older adults demonstrated higher expression of *NOP14* (Fig. 2F), and *NOP14* expression was higher in patients with a dead outcome regarding overall survival (OS). Furthermore, consistent findings were observed when analyzing the Chinese Glioma Genome Atlas (CGGA)-based data (**Supplementary Fig. 1A–D**).

To assess the prognostic value of *NOP14* in GBM patients, the study analyzed the correlation between *NOP14*

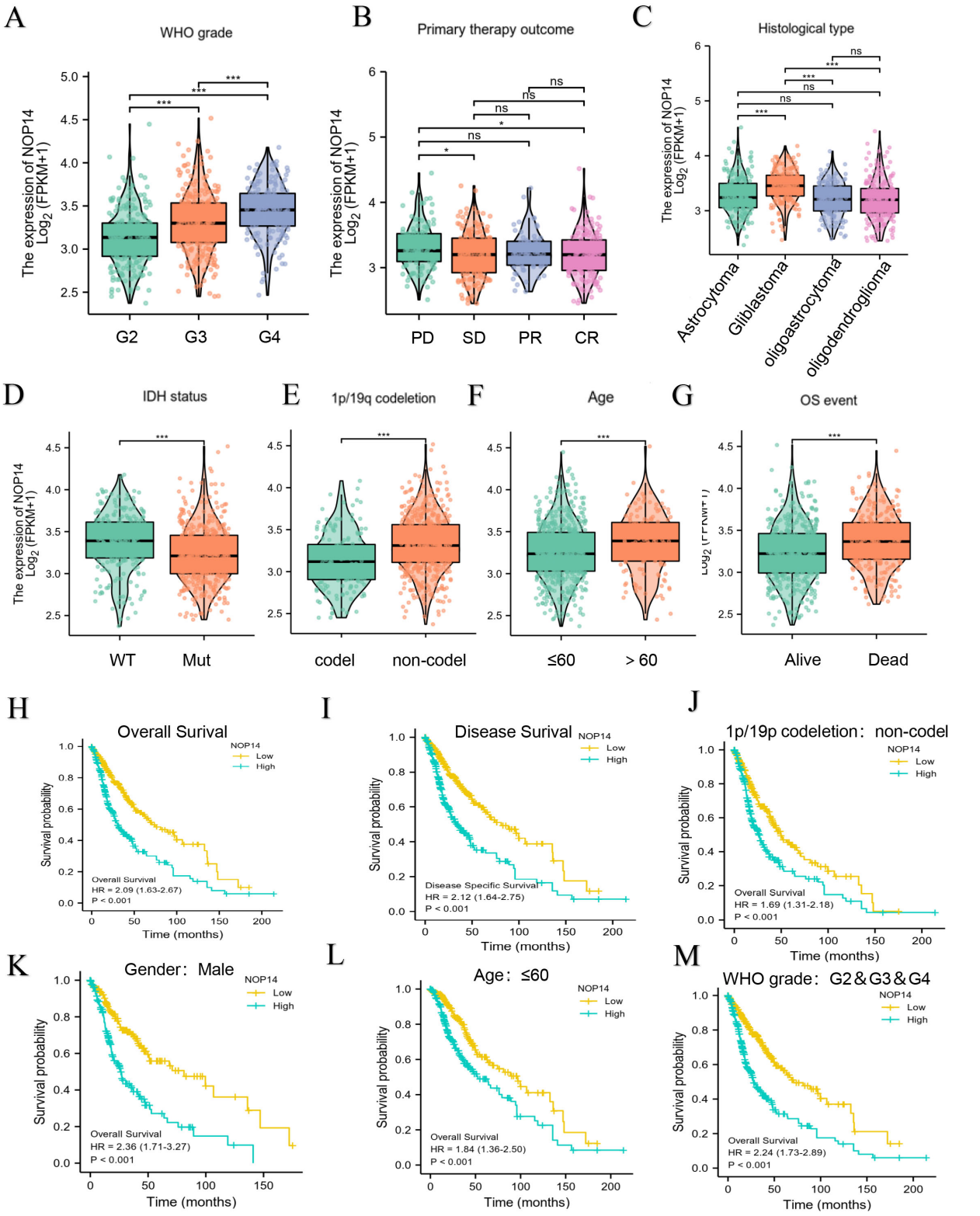

Fig. 2. Correlation between *NOP14* expression and different clinicopathological features and the prognostic value of *NOP14* in OS and DSS of GBM. Correlation between (A) *NOP14* expression and WHO GBM grade, (B) primary treatment, (C) histological type, (D) IDH status, (E) 1p/19p cedar, (F) age, and (G) OS events. (H,I) Prognostic value of *NOP14* in the OS and DSS of GBM. (J–M) High expression of *NOP14* in different subgroups was associated with worse OS. OS, overall survival; DSS, disease-specific survival; GBM, glioblastoma. *** $p < 0.001$, * $p < 0.05$, ^{ns} $p \geq 0.05$.

Table 2. Univariate and multivariate analyses of clinical pathological parameters in GBM patients.

Characteristics	Total (N)	Univariate analysis		Multivariate analysis	
		Hazard ratio (95% CI)	*p* value	Hazard ratio (95% CI)	*p* value
WHO grade	634				
G2	223	Reference			
G3	243	2.999 (2.007–4.480)	<**0.001**	1.936 (1.178–3.180)	**0.009**
G4	168	18.615 (12.460–27.812)	<**0.001**	1.795 (0.466–6.908)	0.395
1p/19q codeletion	688				
Codel	170	Reference			
Non-codel	518	4.428 (2.885–6.799)	<**0.001**	1.797 (0.905–3.572)	0.094
Primary therapy outcome	461				
PD	112	Reference			
SD	147	0.440 (0.294–0.658)	<**0.001**	0.399 (0.242–0.659)	<**0.001**
PR	64	0.170 (0.074–0.391)	<**0.001**	0.177 (0.063–0.500)	**0.001**
CR	138	0.133 (0.064–0.278)	<**0.001**	0.168 (0.078–0.362)	<**0.001**
TP53	695	1.680 (1.427–1.978)	<**0.001**	1.811 (1.283–2.558)	<**0.001**
Age	695	1.066 (1.056–1.076)	<**0.001**	1.064 (1.046–1.082)	<**0.001**
IDH status	685				
WT	246	Reference			
Mut	439	0.117 (0.090–0.152)	<**0.001**	0.427 (0.250–0.731)	**0.002**
Histological type	695				
Glioblastoma	168	Reference			
Oligodendroglioma	198	0.085 (0.060–0.122)	<**0.001**	0.444 (0.234–0.843)	**0.013**
Astrocytoma	195	0.147 (0.107–0.203)	<**0.001**	0.683 (0.399–1.168)	0.164
Oligoastrocytoma	134	0.097 (0.064–0.147)	<**0.001**		
NOP14	695				
Low	348	Reference			
High	347	2.088 (1.632–2.671)	<**0.001**	0.530 (0.329–0.852)	**0.009**

Bold values were statistically significant.

Table 3. *NOP14* expression correlated with clinicopathological characteristics analyzed by logistic regression.

Characteristics	Total (N)	Odds ratio (OR)	*p* value
WHO grade (G3&G4 *vs.* G2)	635	4.040 (2.857–5.765)	<0.001
1p/19q codeletion (non-codel *vs.* codel)	689	3.016 (2.093–4.398)	<0.001
Primary therapy outcome (PR&CR *vs.* PD&SD)	462	0.749 (0.514–1.089)	0.132
IDH status (Mut *vs.* WT)	686	0.334 (0.240–0.461)	<0.001
Histological type (Glioblastoma&Oligoastrocytoma&Oligodendroglioma *vs.* Astrocytoma)	696	1.239 (0.890–1.728)	0.206
Age (>60 *vs.* ≤60)	696	2.347 (1.604–3.471)	<0.001

expression with OS and disease-specific survival (DSS). The findings revealed that high *NOP14* mRNA expression implied a significant association with shorter OS and DSS in the TCGA cohort (OS: hazard ratio [HR] = 2.09, 95% CI = 1.63–2.67, $p < 0.001$; DSS: HR = 2.12, 95% CI = 1.64–2.75, $p < 0.001$) (Fig. 2H,I). Similar results were observed in the CGGA-based data and the PrognoScan database (Fig. 2E,F). Additionally, high *NOP14* mRNA expression showed linkage with shorter OS (Fig. 2G) only in WHO grade 3 gliomas (**Supplementary Fig. 1 E,F**). Besides, patients with lp/19 non-codel, male gender, and age 60 showed a higher expression of *NOP14* mRNA and were associated with shorter OS (Fig. 2J–L). Moreover, higher expression of *NOP14* mRNA in WHO G2, G3, and G4 gliomas was also correlated with shorter OS (Fig. 2M). In conclusion, *NOP14* is significantly upregulated in glioma and is strongly linked to prognosis.

3.4 Associations between NOP14 Expression and Clinicopathologic Variables

The results of the univariate Cox regression analysis uncovered that high expression of *NOP14* showed a linkage with increased risk among adverse clinical prognostic factors (Table 2). Significant variables discovered in the univariate analysis were subsequently included in the multivariate Cox regression analysis. It was evident that *NOP14* expression was an independent risk factor for overall survival (HR: 0.530, $p = 0.009$), thus indicating a predictive value for overall survival in the disease. Moreover, the WHO grade, particularly in the G3 stage, IDH status,

Table 4. Signaling pathways most significantly associated with *NOP14* expression.

Characteristic	Description	NES	*p*-value	*p*.adjust
Positive REACTOME term	REACTOME_CELL_CYCLE	4.773	0.003	0.006
	REACTOME_CELL_CYCLE_MITOTIC	4.698	0.002	0.006
	REACTOME_CELL_CYCLE_CHECKPOINTS	4.427	0.002	0.005
	REACTOME_M_PHASE	4.098	0.002	0.005
	REACTOME_RHO_GTPASE_EFFECTORS	3.570	0.002	0.005
Negative REACTOME term	REACTOME_NEURONAL_SYSTEM	–4.045	0.001	0.005
	REACTOME_TRANSMISSION_ACROSS_CHEMICAL_SYNAPSES	–3.563	0.001	0.005
	REACTOME_NEUROTRANSMITTER_RECEPTORS_AND_POSTSYNAPTIC_SIGNAL_TRANSMISSION	–3.247	0.001	0.005
	REACTOME_SIGNALING_BY_GPCR	–3.0123	0.001	0.005
	REACTOME_TRANSPORT_OF_SMALL_MOLECULES	–2.7192	0.001	0.005
Positive KEGG term	KEGG_CELL_CYCLE	3.002	0.002	0.005
	KEGG_ECM_RECEPTOR_INTERACTION	2.885	0.002	0.005
	KEGG_CYTOKINE_CYTOKINE_RECEPTOR_INTERACTION	2.550	0.002	0.005
	KEGG_FOCAL_ADHESION	2.426	0.002	0.005
	KEGG_P53_SIGNALING_PATHWAY	2.395	0.002	0.005
Negative KEGG term	KEGG_NEUROACTIVE_LIGAND_RECEPTOR_INTERACTION	–4.004	0.001	0.005
	KEGG_CALCIUM_SIGNALING_PATHWAY	–2.825	0.001	0.005
	KEGG_AMYOTROPHIC_LATERAL_SCLEROSIS_ALS	–2.343	0.003	0.006
	KEGG_LONG_TERM_POTENTIATION	–2.216	0.001	0.005
	KEGG_OLFACTORY_TRANSDUCTION	–1.967	0.005	0.009

NES, normalized enrichment score; KEGG, Kyoto Encyclopedia of Genes and Genomes.

histological type, and TP53, demonstrated a predictive advantage for the clinical outcome (Fig. 3A). The results of the univariate logistic regression analysis revealed significant clinicopathological differences between the groups, including WHO grade (odds ratio [OR] = 4.040, 95% CI = 2.857–5.765), 1p/19q codeletion (OR = 3.016, 95% CI = 2.093–4.398), IDH status (OR = 0.334, 95% CI = 0.240–0.461), and age (OR = 2.347, 95% CI = 1.604–3.471) (all $p < 0.001$) (Table 3).

Fig. 3B displays the distribution of *NOP14* expression, the survival status of GBM patients, and the *NOP14* expression profiles. The group with a low-risk score showed a low expression of the dashed line, while the group with a high-risk score exhibited a high expression of the dashed line. With an increase in the risk score of GBM patients, there was a gradual rise in the number of green points, indicating an escalation in the mortality rate among GBM patients. This indicates the survival rate and high risk.

There receiver operating characteristic curve (ROC) curve for the *NOP14* score demonstrated its diagnostic accuracy with an Area Under Curve (AUC) of 0.814 (95% CI = 0.793–0.835) (Fig. 3C). The accuracy of this study was also assessed over time to evaluate the predictive capability of *NOP14* for overall survival at 1, 2, and 3 years (Fig. 3D).

3.5 Functional Enrichment Analysis of Differentially Expressed Genes (DEGs)

In the *NOP14* group, a total of 5892 genes showed differential expression, with 3126 DEGs upregulated (53.0%) and 2766 DEGs downregulated (46.9%) (adjusted *p*-value < 0.05, $\log_2$ fold change $|\text{Log}_2\text{-FC}| > 2$) (**Supplementary Fig. 2A**). The Gene Ontology (GO) analysis revealed that DEG-related *NOP14* significantly regulated various biological processes, including neurotransmitter transport, regulation of postsynaptic membrane potential, calcium ion-regulated exocytosis, ion channel complex formation, synaptic membrane function, substrate-specific channel activity, ion-gated channel activity, and neuroactive ligand-receptor interaction (Fig. 4A, Table 2). The heat map illustrates the correlation between *NOP14* and the 15 genes, as demonstrated in Fig. 4B.

To further elucidate the biological function of *NOP14*, GSEA was implemented on the disparities between the high and low expression datasets of *NOP14* (Table 4). This analysis enabled us to identify the specific REACTOME and KEGG pathways associated with *NOP14*. Besides, 244 pathways exhibited significant differences in the enrichment of the REACTOME and KEGG pathways in the samples with high *NOP14* expression (FDR <0.05, adjusted $p < 0.05$). Table 3 displays the REACTOME and KEGG pathways that are significantly enriched based on NES. The GSEA analysis of the REACTOME depicted that high levels of *NOP14* were positively correlated with various aspects of the cell cycle, such as cell cycle progression, mitotic division, and cell cycle checkpoint regulation, as well as with M phase and RHO GTPase effectors (Fig. 4C). On the other hand, high levels of *NOP14* were negatively correlated with neuronal system function, chemical synapse

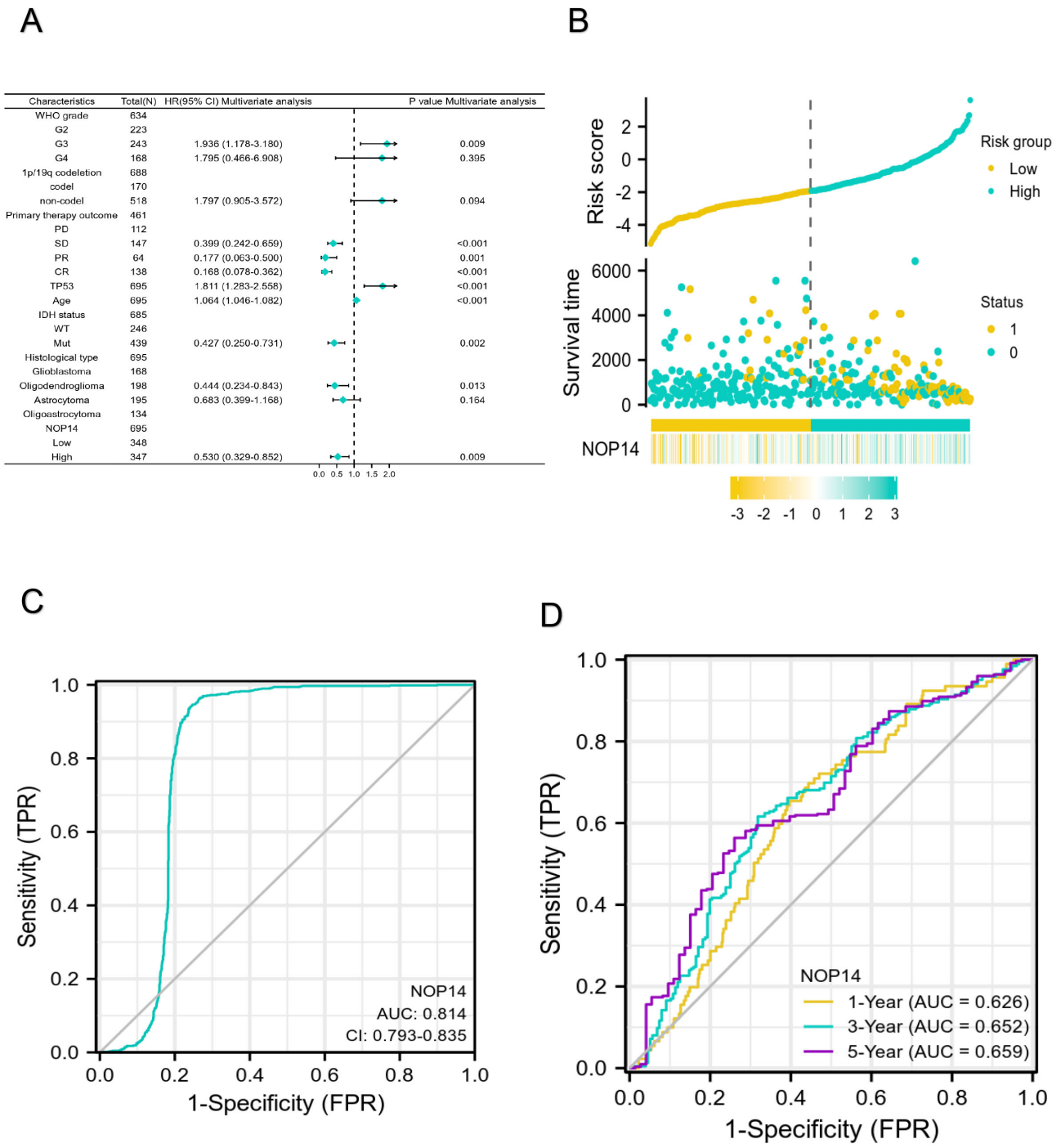

Fig. 3. The prognostic value of *NOP14* in GBM. (A) Multivariate Cox regression visualized in the forest plot. (B) *NOP14* expression distribution and survival status. 0: dead, 1: alive. (C) Diagnostic receiver operating characteristic curve (ROC) curve of *NOP14*. (D) Time-dependent ROC curve of *NOP14*.

transmission, neurotransmitter receptor activity, postsynaptic signal transmission, and G Protein-Coupled Receptor signaling (Fig. 4D). A GSEA of the KEGG pathway revealed significant enrichment in several pathways, including the Cell Cycle, Cytokine-Cytokine Receptor Interaction, Focal Adhesion, ECM Receptor Interaction, and P53 Pathway, which exhibited a positive correlation with high levels of *NOP14* (Fig. 4E). On the other hand, the following pathways were found to be negatively correlated with high levels of *NOP14*: Neuroactive ligand-receptor interaction, Calcium signaling pathway, Amyotrophic lateral sclerosis, Long-term potentiation, Olfactory transduction, and PPAR signaling pathways (Fig. 4F). Our findings indicate a strong association between *NOP14* expression and neural conduction, cell cycle control, and cytokine receptor interactions.

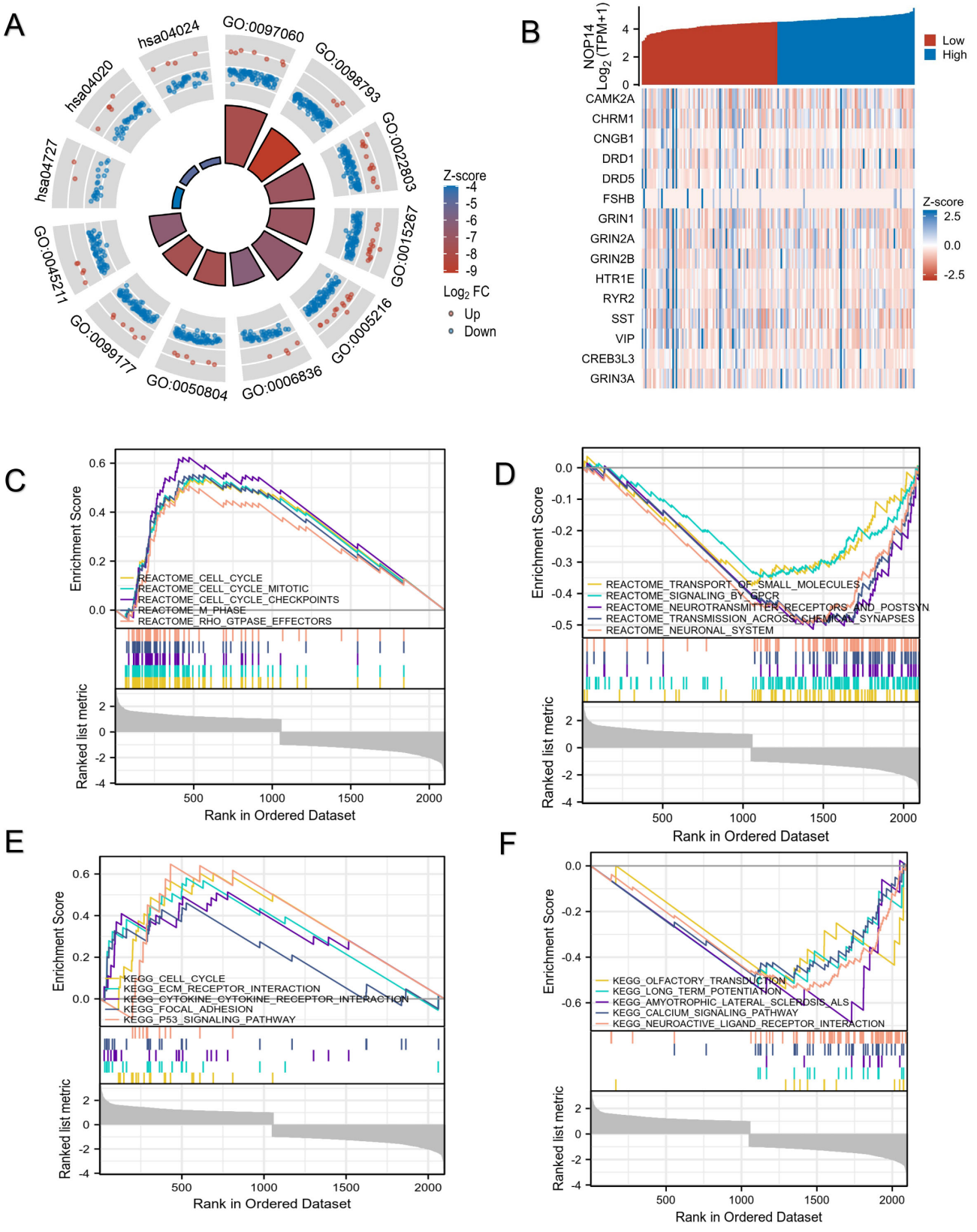

Fig. 4. Enrichment analysis of *NOP14* in GBM. (A) Biological process enrichment related to *NOP14*-related genes. (B) A network of *NOP14* and its 20 potential co-interaction proteins. (C–F) The results of enrichment analysis from GSEA. GSEA, Gene Set Enrichment Analysis.

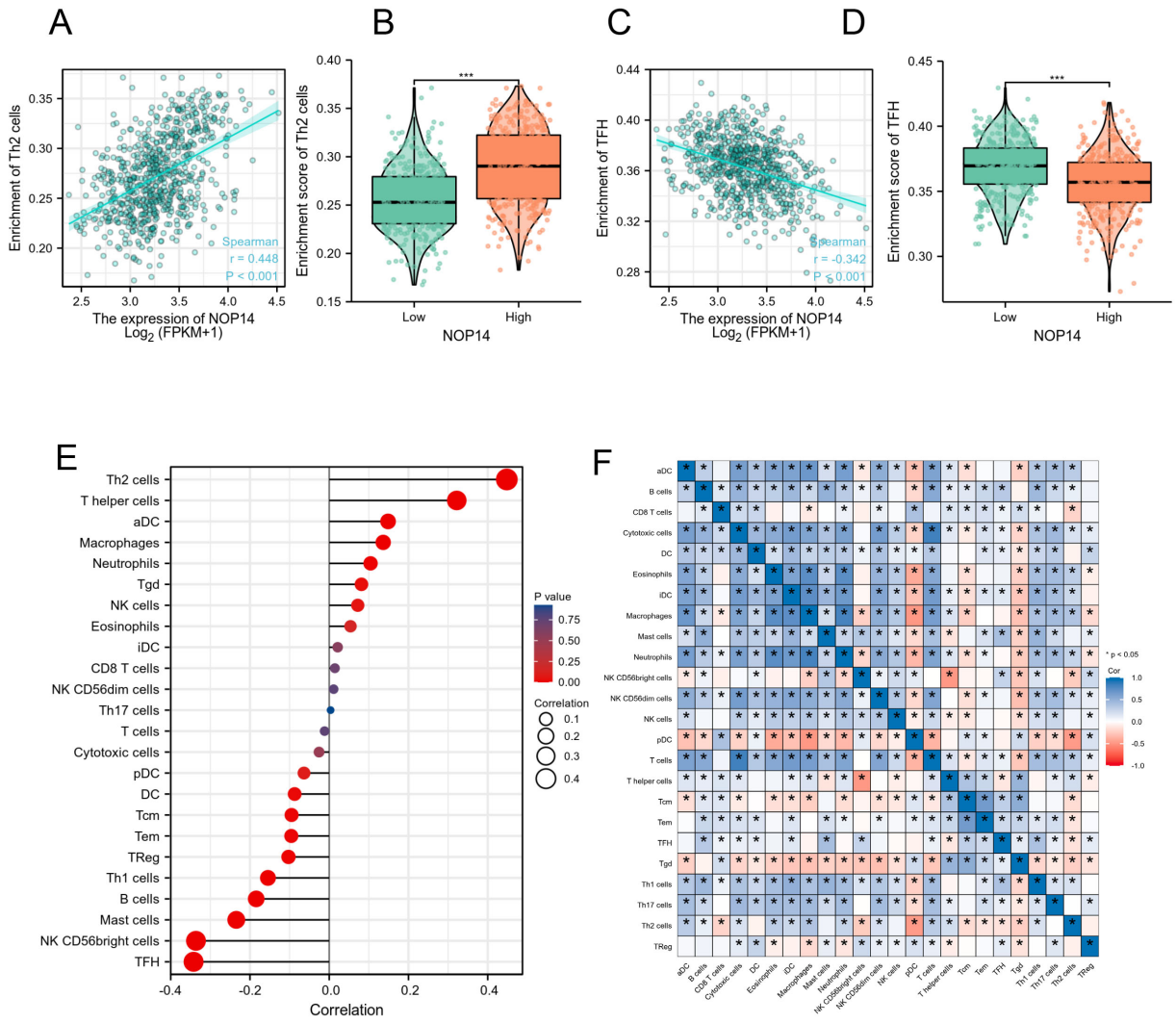

Fig. 5. The results of analysis between *NOP14* expression and immune infiltration. (A) The positive correlation between *NOP14* expression and Th2 cells. (B) Th2 cells' infiltration level in different *NOP14* expression groups. (C) The negative correlation between *NOP14* expression and Follicular helper T cell (TFH). (D) TFH'infiltration level in different *NOP14* expression groups. (E) Correlation between *NOP14* expression level and the relative abundances of 24 immune cells. (F) Heat map of 24 immune infiltration cells in GBM. ***, $p < 0.001$.

3.6 Relationship between NOP14 Expression and Immune Infiltration

A Spearman correlation analysis was implemented to investigate the relationship between *NOP14* and the levels of immune cell infiltration, quantified by the ssGSEA score. The infiltration level of Th2 cells was positively correlated with *NOP14* expression (Spearman's R = 0.448) (Fig. 5A) and was elevated in the high *NOP14* expression group (all $p < 0.001$) (Fig. 5B). Conversely, follicular helper T cells (Tfh) exhibited a negative correlation with *NOP14* expression (Spearman's R = –0.342) (Fig. 5C), and *NOP14* expression declined in the high *NOP14* expression group (all $p < 0.001$) (Fig. 5D). Th2 cells, T helper cells, aDC, macrophages, neutrophils, Tgd, NK cells, and eosinophils exhibited a positive relationship with *NOP14*. Besides, a negative correlation existed between TFH, NK, CD56bright cells, mast cells, B cells, Th1 cells, TReg, Tem, Tcm, pDC, DC, and *NOP14* (Fig. 5E). Thus, *NOP14* plays a significant role in the immune infiltration of GBM. The heatmap was used to assess and observe the varying degrees of correlation between the proportions of the 24 types of tumor-infiltrating immune cell subsets (Fig. 5F).

3.7 Association of NOP14 Levels with Immune Cell Infiltration

Research has demonstrated that relying solely on clinicopathological characteristics does not yield accurate prognostic information for tumor patients, resulting in excessive or inadequate treatment. Emerging evidence indicates that incorporating tumor microenvironment (TME)-related immune scores and the proportion of tumor-infiltrating immune cells (TIC) in the TME can enhance the predictive

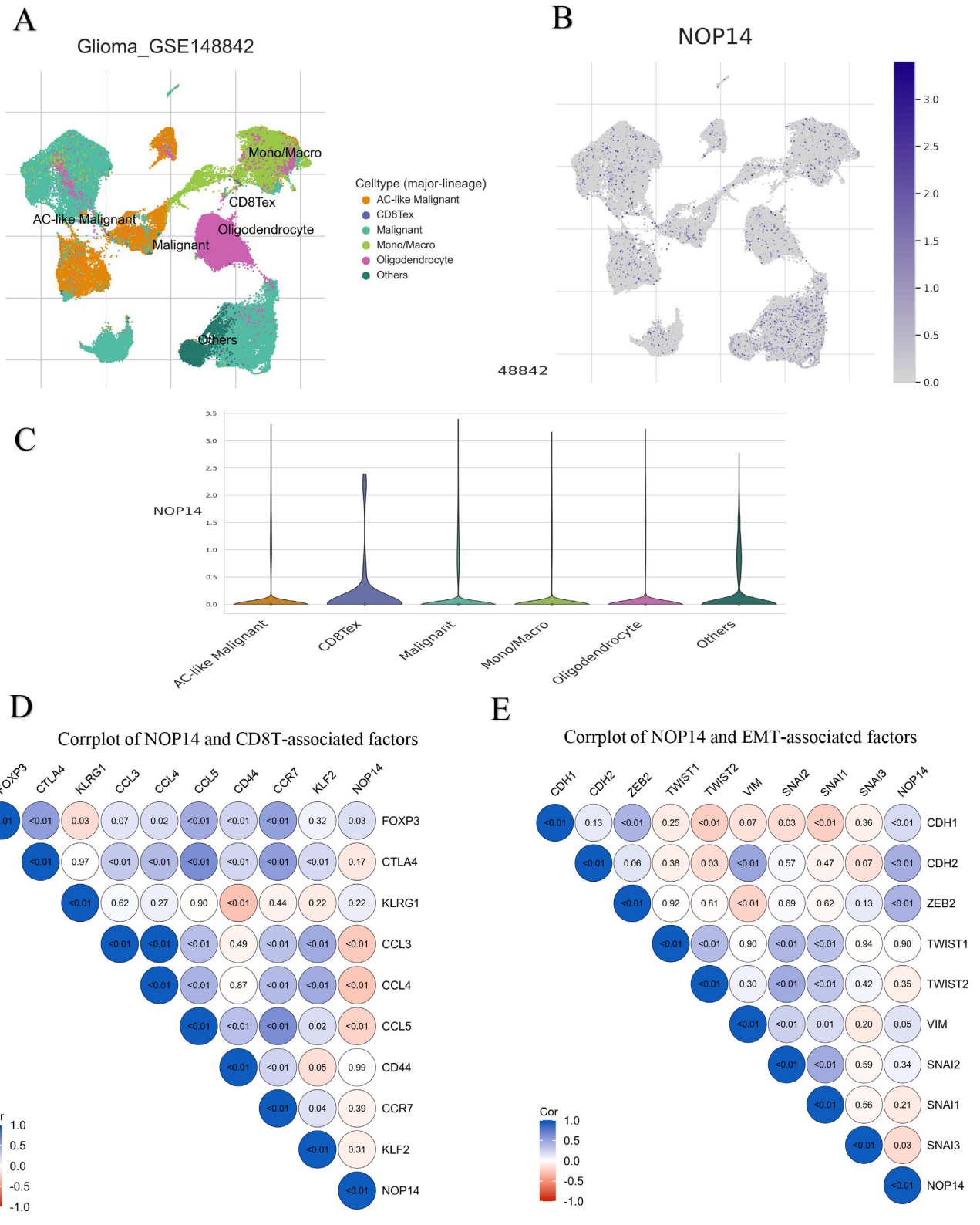

Fig. 6. Correlation between *NOP14* levels and stromal cell infiltration. (A–E) GFPT2 was expressed in both immune and stromal cell single-cell subpopulations in a Glioma single-cell GSE dataset (GSC_GSE148842_Smartseq2) from the Tumor Immune Single-cell Hub (TISCH) dataset. (D) Corrplot was used to perform the correlation between *NOP14* levels and CD8T-associated factors. (E) A corrplot was used to perform the correlation between *NOP14* levels and EMT-related factors.

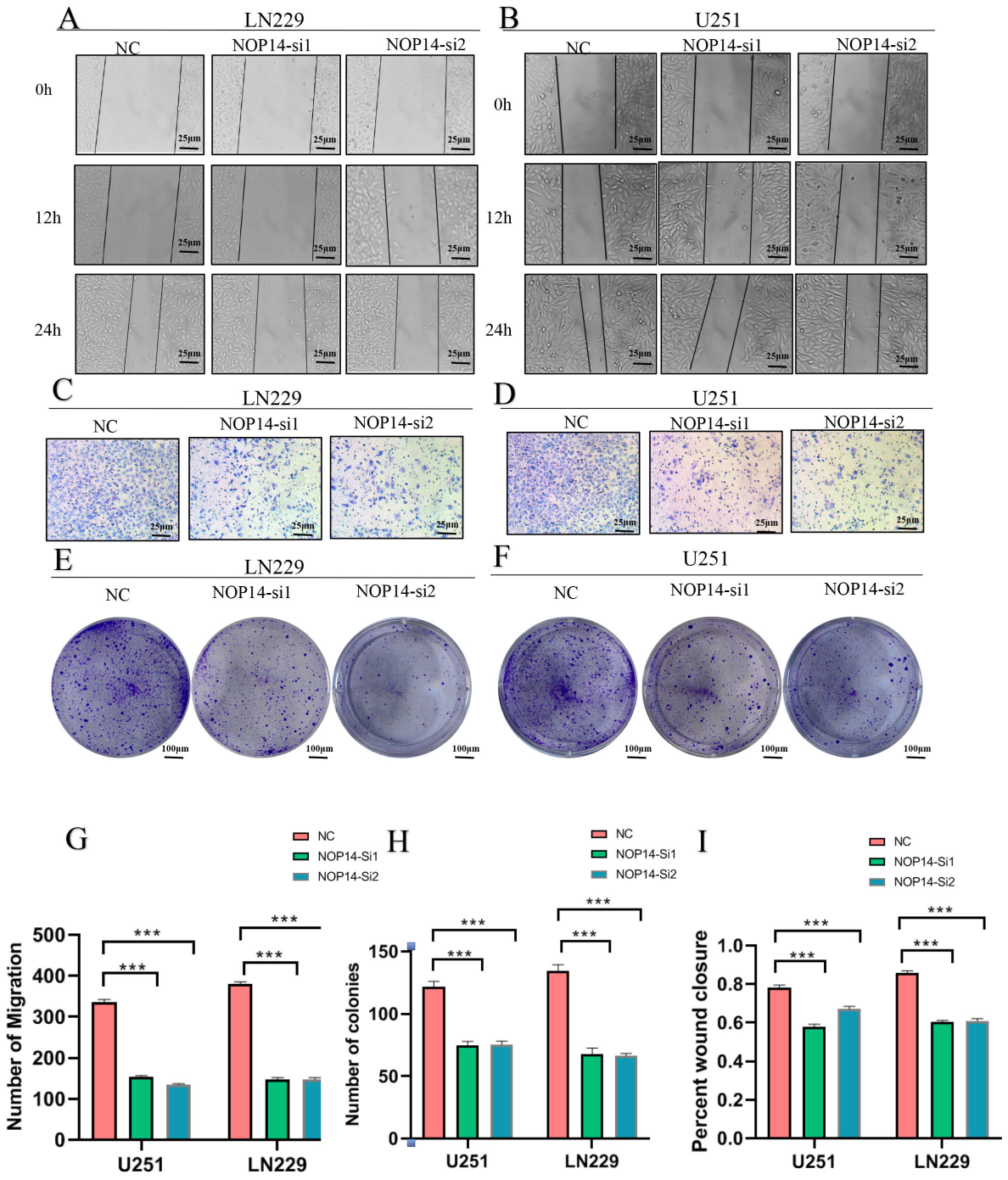

Fig. 7. *NOP14* promotes glioma cell migration and invasion *in vitro*. (A,B) Images of wound healing experiments in the NC and *NOP14* gene interference groups. (G) Quantification of the wound closure condition. (C,D) Images of migrated transwell experiments in NC and *NOP14* gene interference groups. (H) Quantitative analysis of the number of migrating glioma cells. (E,F) Plate cloning experiments of the NC and *NOP14* gene interference groups. (I) Quantitative analysis of the plate clones. *** $p < 0.001$.

accuracy of conventional staging systems [11–14]. TME comprises tumor cells, stromal cells, immune cells, extracellular matrix (ECM), signaling molecules, and cytokines. Immune cells in the TME can influence tumor growth [15–17]. To explore the association between *NOP14* levels and stromal cell infiltration, we initially analyzed the Tumor Immune Single Cell Center [13] database to determine the main cell subset expressing *NOP14*. The GSC_GSE148842_Smartseq2 dataset (a glioma single-cell dataset) was explored. We discovered the expression of *NOP14* in both single-cell subsets of immune and stromal cells (Fig. 6A–C). Subsequently, we examined the specific cell subsets of *NOP14* species exhibiting high glioma expression. The results demonstrated that $CD8^+$Tex cells pre-

dominantly expressed *NOP14*. Additionally, *NOP14* exhibited higher expression in $CD8^+$Tex cells than other cell subsets (Fig. 4C). These findings strongly clarify the pivotal role of *NOP14* in modulating the functions of $CD8^+$Tex cells.

We further pinpointed the correlation between *NOP14* and biomarkers linked to $CD8^+$T cells. $CD8^+$ tumor-infiltrating lymphocytes ($CD8^+$TILs) are the primary immune cell population responsible for tumor eradication. However, numerous studies indicate that continuous antigen stimulation in the TME, along with the presence of immunosuppressive factors, leads to the progressive exhaustion of $CD8^+$T cells. Consequently, the functions of these exhausted $CD8^+$T cells, including their ability to kill tumors and proliferate, gradually diminish, eventually resulting in their complete functional loss [18]. Functional identification of killing T cells can be based on various physiological states. For instance, effector T cell cytokines such as CCL3 (MIP-1α), CCL4 (MIP-1β), CCL5 (RANTES), effector memory T cell surface markers including CD44, low expression of CD197 (CCR7), and KLRG1, and the tissue-resident memory T-cell transcription factor KLF2 can be used. Studies have shown that CTLA-4 can suppress CD28 co-stimulatory signals by binding to B7 molecules, thereby inhibiting the activation of CD8T cells [19,20]. Our study noted a strong negative correlation between *NOP14* and the $CD8^+$T marker genes *CCL3*, *CCL4*, and *CCL5*. Additionally, we found a positive correlation between *NOP14* expression and forkhead box protein 3 (Foxp3) (Fig. 6D).

$CD8^+$Tex bears great responsibility for tumor development, and the synergistic effects of these inhibitory features induce Epithelial–mesenchymal transition (EMT) and impact tumor cell survival [21]. To validate the impact of *NOP14* expression on EMT, we investigated the correlation between *NOP14* levels and EMT-associated markers. The findings indicated a strong correlation between *NOP14* expression and EMT-related factors (Fig. 6E). These findings unveil that *NOP14* could serve as a potential biomarker for modifications in the tumor immune microenvironment, especially those related to $CD8^+$T cells.

3.8 NOP14 Facilitates the Migration and Proliferation of GBM Cells in Vitro

In vitro, interference of *NOP14* was observed in LN229 and U251 cells (**Supplementary Fig. 3A,B**). The cell wound scratch assay demonstrated that the inhibition of *NOP14* resulted in a reduction in cell migration (Fig. 7A,B,G). Similarly, the Transwell assay indicated a decrease in cell invasion upon reduction of *NOP14* expression (Fig. 7C,D,H). Furthermore, the clone formation assay provided evidence that the inhibition of *NOP14* impaired the colony formation ability of GBM cells (Fig. 7E,F,I).

4. Discussion

NOP14 promotes localization by interacting with the nucleolar RNA methyltransferase EMG1, thereby playing a pivotal role in the processing of 18s rRNA precursor and assembly of the small ribosomal subunit [6–8]. However, the expression and function of *NOP14* in human malignancies remain poorly understood.

The present study conducted a combined analysis of the CGGA and TCGA databases, revealing a significant upregulation of *NOP14* expression in gliomas. These findings were consistent with the results obtained from the HPAs database. Furthermore, elevated *NOP14* expression was correlated with adverse clinicopathological factors, including non-codel 1p/19q codeletion, WHO grade (G3&G4), Mut subtype of IDH status, age ($p < 0.001$), and histological type ($p < 0.001$). Moreover, our data supported the notion that increased *NOP14* expression could be an autonomous prognostic indicator for unfavorable OS and DSS in patients with adult-type diffuse glioma. The findings suggested that elevated levels of *NOP14* expression exhibited a significant impact on the development and progression of adult-type diffuse glioma. It was observed that *NOP14* expression increased with higher glioma WHO grades, which implied a potential association between *NOP14* and the aggressiveness of adult-type diffuse glioma.

NOP14 participates in a crucial biological process of cellular ribosome synthesis, which may significantly influence the onset and progression of malignancy. Ribosomes are widely acknowledged as the site of protein synthesis in cells [21]. In tumor cells, a substantial quantity of ribosomes is essential to sustain a highly proliferative state and synthesize an adequate amount of proteins for various cellular physiological activities. Previous studies have demonstrated the involvement of ribosomes in DNA damage repair, cell cycle regulation, and proliferation, and dysfunctional ribosomes can contribute to cell transformation and tumor progression [22–24]. To enhance our comprehension of *NOP14*'s involvement in the advancement and evolution of GBM, we performed a GSEA analysis within this research endeavor to elucidate its role in GBM. The GSEA results revealed a positive enrichment of REACTOME terms associated with cell cycle, cell cycle mitotic, cell cycle checkpoints, M phase, and RHO GTPase effectors. Alternatively, the KEGG pathway analysis results suggested that cancer-related pathways, including the cell cycle and P53, exhibited a positive enrichment when *NOP14* was highly expressed. This finding was consistent with the established biological function of *NOP14*, implying that its involvement in cell cycle regulation may contribute to tumor progression in adult-type diffuse glioma. However, further experimental validation is still needed.

In general, immune cells can recognize and remove abnormal tumor cells [25]. However, tumor cells employ various strategies to evade the antitumor response of the

human immune system. Within the TME, stromal cells and immune cells induce alterations such as increased extracellular matrix stiffness, vascular and lymphatic vessel formation, necrotic zone formation, and tumor metastasis through autocrine and paracrine production [26]. Therefore, immune cells play a pivotal role in tumor development. Earlier research has indicated a link between heightened *NOP14* expression in PDAC and localized metastasis and lymphatic invasion [10]. Here, we observed a negative correlation between the expression of *NOP14* and the levels of various immune cells, including TFH, NK CD56bright cells, mast cells, B cells, Th1 cells, Treg cells, Tem cells, Tcm cells, pDCs, and DCs. Diminished Tfh cells in the TME resulted in imbalanced humoral immunity and the inactivation of natural killer (NK) cells. As a consequence, the anti-tumor capacity is compromised. It is strongly linked to the formation of an immunosuppressive microenvironment within Glioma [27]. Glioma cells and other immune-regulatory-related cells, such as DC, present in the TME, are capable of producing and releasing cytokines, including transforming growth factor, IL-6, IL-10, prostaglandin E2, and ID-2,3-dioxygenase, which have the potential to directly or indirectly suppress the activation of NK cells [28]. Drawing from these findings, one could infer that the significant *NOP14* overexpression was vital in governing ribosome production and cell cycle control in adult-type diffuse glioma. Additionally, *NOP14* may act as a potential immune modulator, inhibiting glioma immune infiltration.

The single-cell transcriptome analysis provides insights into tumor heterogeneity and holds great potential for individualized therapy [29]. To gain a deeper understanding of the mechanisms underlying adult-type diffuse glioma progression and its response to immunotherapy, we investigated the involvement of specific genes in tumor EMT and $CD8^+$T cell infiltration. Our study unveiled a notable inverse relationship between *NOP14* expression and tumor infiltration of $CD8^+$T cells. Furthermore, *NOP14* was highly abundant in the $CD8^+$T cell exhaustion subtype. There is growing evidence suggesting that depleted $CD8^+$T cells experience metabolic dysfunction, resulting in alterations in signaling cascades and epigenetic profiles. This leads to the suppression of effector immunity and ultimately hampers the response to immune checkpoint blockade therapy [30,31]. The restoration of depleted $CD8^+$T cells' anti-tumor activity through reducing *NOP14* expression is an emerging field with the potential to enhance the response rate of immunotherapy. However, further studies are required to confirm this.

5. Conclusions

In conclusion, the results demonstrate the potential of *NOP14* as a prognostic biomarker and an indicator for immunotherapy. Furthermore, our study demonstrated a close association between *NOP14* and cell migration and proliferation of adult-type diffuse glioma *in vitro*, highlighting the potential impact of *NOP14* on adult-type diffuse glioma development and prognosis. However, further validation *in vivo* is still required in our future studies.

Availability of Data and Materials

All data analyzed in this review are included in this article and/or its figures. Further inquiries can be directed to the corresponding author.

Author Contributions

QST performed the experiments, collected all the relevant data, and wrote the first draft of this manuscript with most figures and supplemental information. JC performed the histological examination. ZJB designed and supervised this study, analyzed all the data, helped to prepare all figures with cartoons, and rewrote and revised the paper. All authors contributed to editorial changes in the manuscript. All authors have read and agreed to the published version of the manuscript. All authors have participated sufficiently in the work and agreed to be accountable for all aspects of the work.

Ethics Approval and Consent to Participate

This study was approved by the Ethics Committee of 3201 Hospital (approval number 2022082). Helsinki declaration has been followed for involving human subjects in the study, and relevant guidelines for animal experimentation have been followed. Signed written informed consents were obtained from all participants before the study.

Acknowledgment

Not applicable.

Funding

This study was funded by the General Medical Research Fund (TYYLKYJJ-2022-014).

Conflict of Interest

The authors declare no conflict of interest.

Supplementary Material

Supplementary material associated with this article can be found, in the online version, at https://doi.org/10.31083/j.fbl2903104.

References

[1] Xu S, Tang L, Li X, Fan F, Liu Z. Immunotherapy for glioma: Current management and future application. Cancer Letters. 2020; 476: 1–12.

[2] Liang S, Fan X, Zhao M, Shan X, Li W, Ding P, *et al*. Clinical practice guidelines for the diagnosis and treatment of adult diffuse glioma-related epilepsy. Cancer Medicine. 2019; 8: 4527–4535.

[3] Nicholson JG, Fine HA. Diffuse Glioma Heterogeneity and Its

Therapeutic Implications. Cancer Discovery. 2021; 11: 575–590.
[4] Liu PC, Thiele DJ. Novel stress-responsive genes EMG1 and NOP14 encode conserved, interacting proteins required for 40S ribosome biogenesis. Molecular Biology of the Cell. 2001; 12: 3644–3657.
[5] Milkereit P, Strauss D, Bassler J, Gadal O, Kühn H, Schütz S, *et al*. A Noc complex specifically involved in the formation and nuclear export of ribosomal 40 S subunits. The Journal of Biological Chemistry. 2003; 278: 4072–4081.
[6] Kühn H, Hierlmeier T, Merl J, Jakob S, Aguissa-Touré AH, Milkereit P, *et al*. The Noc-domain containing C-terminus of Noc4p mediates both formation of the Noc4p-Nop14p submodule and its incorporation into the SSU processome. PLoS ONE. 2009; 4: e8370.
[7] Du Y, Liu Z, You L, Hou P, Ren X, Jiao T, *et al*. Pancreatic Cancer Progression Relies upon Mutant p53-Induced Oncogenic Signaling Mediated by NOP14. Cancer Research. 2017; 77: 2661–2673.
[8] Meng T, Lan Z, Zhao X, Niu L, Chen C, Zhang W. Comprehensive bioinformatics analysis of functional molecules in colorectal cancer. Journal of Gastrointestinal Oncology. 2022; 13: 231–245.
[9] Gusyatiner O, Hegi ME. Glioma epigenetics: From subclassification to novel treatment options. Seminars in Cancer Biology. 2018; 51: 50–58.
[10] Gong L, Huang D, Shi Y, Liang Z, Bu H. Regulated cell death in cancer: from pathogenesis to treatment. Chinese Medical Journal. 2023; 136: 653–665.
[11] Sun D, Wang J, Han Y, Dong X, Ge J, Zheng R, *et al*. TISCH: a comprehensive web resource enabling interactive single-cell transcriptome visualization of tumor microenvironment. Nucleic Acids Research. 2021; 49: D1420–D1430.
[12] Ying Y, Li J, Xie H, Yan H, Jin K, He L, *et al*. CCND1, NOP14 and DNMT3B are involved in miR-502-5p-mediated inhibition of cell migration and proliferation in bladder cancer. Cell Proliferation. 2020; 53: e12751.
[13] Lei JJ, Peng RJ, Kuang BH, Yuan ZY, Qin T, Liu WS, *et al*. NOP14 suppresses breast cancer progression by inhibiting NRIP1/Wnt/β-catenin pathway. Oncotarget. 2015; 6: 25701–25714.
[14] Li J, Fang R, Wu J, Si Y, Bai J, Wang Q. The NOP14 nucleolar protein suppresses the function and stemness of melanoma stem-like cells through Wnt/beta-catenin signaling inactivation. Bioengineered. 2022; 13: 7648–7658.
[15] Ma Y, Xi Z. Integrated Analysis of Multiomics Data Identified Molecular Subtypes and Oxidative Stress-Related Prognostic Biomarkers in Glioblastoma Multiforme. Oxidative Medicine and Cellular Longevity. 2022; 2022: 9993319.
[16] Dhanasekaran R, Suzuki H, Lemaitre L, Kubota N, Hoshida Y. Molecular and immune landscape of hepatocellular carcinoma to guide therapeutic decision making. Hepatology (Baltimore, Md.). 2023. (online ahead of print)
[17] Hegde PS, Chen DS. Top 10 Challenges in Cancer Immunotherapy. Immunity. 2020; 52: 17–35.
[18] McLane LM, Abdel-Hakeem MS, Wherry EJ. CD8 T Cell Exhaustion During Chronic Viral Infection and Cancer. Annual Review of Immunology. 2019; 37: 457–495.
[19] Jia SN, Han YB, Yang R, Yang ZC. Chemokines in colon cancer progression. Seminars in Cancer Biology. 2022; 86: 400–407.
[20] Gause WC, Rothlin C, Loke P. Heterogeneity in the initiation, development and function of type 2 immunity. Nature Reviews.Immunology. 2020; 20: 603–614.
[21] Khan M, Ai M, Du K, Song J, Wang B, Lin J, *et al*. Pyroptosis relates to tumor microenvironment remodeling and prognosis: A pan-cancer perspective. Frontiers in Immunology. 2022; 13: 1062225.
[22] Ruggero D, Pandolfi PP. Does the ribosome translate cancer? Nature Reviews. Cancer. 2003; 3: 179–192.
[23] Montanaro L, Treré D, Derenzini M. Changes in ribosome biogenesis may induce cancer by down-regulating the cell tumor suppressor potential. Biochimica et Biophysica Acta. 2012; 1825: 101–110.
[24] Montanaro L, Treré D, Derenzini M. Nucleolus, ribosomes, and cancer. The American Journal of Pathology. 2008; 173: 301–310.
[25] Parkin J, Cohen B. An overview of the immune system. Lancet (London, England). 2001; 357: 1777–1789.
[26] Roma-Rodrigues C, Mendes R, Baptista PV, Fernandes AR. Targeting Tumor Microenvironment for Cancer Therapy. International Journal of Molecular Sciences. 2019; 20: 840.
[27] Perng P, Lim M. Immunosuppressive Mechanisms of Malignant Gliomas: Parallels at Non-CNS Sites. Frontiers in Oncology. 2015; 5: 153.
[28] Terrén I, Orrantia A, Vitallé J, Zenarruzabeitia O, Borrego F. NK Cell Metabolism and Tumor Microenvironment. Frontiers in Immunology. 2019; 10: 2278.
[29] Eisenbarth D, Wang YA. Glioblastoma heterogeneity at single cell resolution. Oncogene. 2023; 42: 2155–2165.
[30] Lee J, Nicosia M, Hong ES, Silver DJ, Li C, Bayik D, *et al*. Sex-Biased T-cell Exhaustion Drives Differential Immune Responses in Glioblastoma. Cancer Discovery. 2023; 13: 2090–2105.
[31] Liu F, Zhou Q, Jiang HF, Zhang TT, Miao C, Xu XH, *et al*. Piperlongumine conquers temozolomide chemoradiotherapy resistance to achieve immune cure in refractory glioblastoma via boosting oxidative stress-inflamation-CD8$^+$-T cell immunity. Journal of Experimental & Clinical Cancer Research: CR. 2023; 42: 118.